

GT2011-45497

A QUASI-ONE-DIMENSIONAL CFD MODEL FOR MULTISTAGE COMPRESSORS

W. Du

University of Liège
Turbomachinery Group
B-4000 Liège, Belgium
Institute of Engineering Thermophysics
Chinese Academy of Sciences, China
wenhai.du@student.ulg.ac.be

O. Léonard

University of Liège
Turbomachinery Group
Chemin des chevreuils 1
B-4000 Liège, Belgium
o.leonard@ulg.ac.be

ABSTRACT

In this contribution a quasi-one-dimensional tool for stationary and transient simulations of post-stall flows in multistage axial compressors is presented. An adapted version of the 1D Euler equations with additional source terms is discretized with a finite volume method and solved in time by a fourth-order Runge-Kutta scheme. The equations are discretized at mid-span both inside the blade rows and the non-bladed regions. The source terms express the blade-flow interactions and are estimated by calculating the velocity triangles for each blade row. Several loss and deviation correlations are implemented and compared to experimental data in normal flow, stalled flow and reversed flow regions.

Transient simulations are carried out and a parameter study is presented to analyze the shape of the surge cycles and the frequency of the surge oscillations. At last, a bleeding control strategy is implemented to study the recoverability of the instabilities in a compression system.

Keywords: surge, axial compressor, dynamic simulation, quasi-one-dimensional model, bleeding control

NOMENCLATURE

a speed of sound
 A flow section area
 b blockage factor
 B non-dimensional number
 E specific internal energy

F force term
 H specific enthalpy
 i incidence angle
 K_{out} throttle coefficient
 L effective length of equivalent duct
 P pressure
 Q source term
 r radius
 SW shaft work
 U rotor velocity
 V_p plenum volume
 V absolute velocity
 W relative velocity
 ρ density
 τ time scale
 ω Helmholtz resonator frequency
 P_{ts} total-to-static pressure coefficient
 $P_{ts} = (P_{s2} - P_{t1}) / (1/2 * \rho * U^2)$ forward flow
 $P_{ts} = (P_{t2} - P_{s1}) / (1/2 * \rho * U^2)$ reversed flow

Subscripts

1 blade leading edge
2 blade trailing edge

Superscripts

0 total conditions

INTRODUCTION

Dynamic simulations of post-stall transients are useful for design purpose and aero-thermodynamic analysis. Many investigations have been carried out through experimental tests and numerical simulations. Experimental tests are not practical for preliminary design purpose. Therefore, in this precise context, time-accurate numerical simulations are suitable for the prediction of the stability boundaries, for the simulation of the post-stall behavior and for studying the control strategy in compression systems.

The prediction tool presented in this contribution is based on an adapted version of Euler equations, mass, axial momentum, circumferential momentum and energy balances being applied on each control volume at mean radius. These equations are solved by a time-marching, finite-volume method [1]. The mesh cells are not only distributed between blade rows, but also inside of each blade row, allowing for a detailed representation of the flow field. The source terms expressing the blade-flow interactions are estimated by determining the velocity triangles for each blade row. Empirical correlations have been incorporated to predict the performance for normal flows, stalled flows and even reversed flows.

The Gamache three-stage low-speed axial compressor is chosen to validate this model [2]. First, steady characteristics predicted using different correlations are compared to the experimental results. Second, transient simulations of the compression system are carried out. The influence of the parameter B (as introduced by Greitzer [4]) and of the throttle setting on the shape of the surge cycles and on the frequency of the surge oscillations are studied and presented. Third, a bleeding device is implemented to study the recoverability of the compression system from stalled conditions.

BACKGROUND

Two kinds of post-stall phenomena, rotating stall and surge, can occur in compression systems [3]. Rotating stall is a severe non-axisymmetric flow which includes one or several stall cells, characterized by lower mass flows and pressure ratios, propagating in the circumferential direction at a fraction of the rotor speed. However, the annulus average mass flow and pressure ratio remain almost constant once the stall cells are fully developed. Surge is an unsteady 1D phenomenon with mass flow oscillations in the axial direction. Surge can be classified according to the amplitude and the frequency of the oscillations.

Classic surge is defined when the flow direction in the compressor remains always positive, while deep surge is characterized by the occurrence of negative flows. Both rotating stall and surge can cause serious damages to the compressor because they can be responsible of high temperatures, vibrations and large stresses on the blades. Meanwhile, due to the non-recoverability of the stall phenomenon, it is also necessary for designers to analyze the

post-stall behavior of the compression system subsequent to the onset of stall.

1D models have been widely applied to study the overall performance of compression systems. Greitzer developed a lumped-volume method to study surge and rotating stall phenomena, based on the compressor steady characteristics [4, 5]. Davis applied a stage-by-stage method with source terms extracted from the steady characteristics and carried out parametric studies [6]. Morini developed a 1D non-linear modular dynamic model to study the transient behavior of compression systems through an imaginary steady-state performance map [7].

On other hand, 2D and 3D models were developed to describe the onset of rotating stall and the global performance in presence of stall cells. Takata and Nagato developed a 2D model to simulate rotating stall in axial compressors, with the assumption that the blade row is replaced by a semi-actuator disk [8]. Moore and Greitzer proposed a 2D, unsteady, lumped parameter model to study the dynamic response of compression systems and the coupling between rotating stall and surge [9]. Longley described a 2D model to simulate instable behaviors, but it could not handle reversed flows [10]. Lindau developed a quasi-3D actuator-disk model to simulate rotating stall and surge in compression systems, with source terms to represent blade losses and deviations [11]. Escuret used 3D Euler equations with source terms estimated from empirical equations; however, it could not simulate reversed flows [12]. Tauveron proposed new empirical correlations to estimate the steady compressor performance in all flow regions, and used them for dynamic simulations [13]. Longley presented a physical-based blockage-mixing method and a novel blockage-transport equation to calculate stall and surge transients, reducing the need for empirical information [14].

Some of the models mentioned above are limited to the instability inception, while many of them cannot handle reversed flows. Meanwhile, most of these models rely on steady compressor maps for all flow regions, which can only be obtained from experimental data or derived from generic performance curves. However, steady characteristics established through rig tests are likely to cover only a part of the compressor domain. On the other hand, steady characteristics generated by simple correlations do not take into account the real geometry of the compressor.

It is therefore worth it to develop an analysis tool to simulate the dynamic performance of a compressor on the sole basis of its geometry. For this purpose empirical correlations have been implemented to predict the steady performance in all flow regions. These empirical correlations are further used to simulate post-stall transients.

GENERAL FORMULATION OF THE MODEL

It is assumed that the flowpath meanline is a streamline and that the flow is axisymmetric.

The quasi-1D Euler equations are set up by the application of conservation principles to each control volume. Radial velocities and angular derivatives are neglected. The fluid is treated as an ideal gas. The mass flow, axial momentum,

circumferential momentum and energy equations can be described in vector, non-dimensional, conservative form, as follows:

$$\frac{\partial U}{\partial t} + \frac{\partial F}{\partial x} = Q \quad (1)$$

$$U = \begin{bmatrix} \rho A \\ \rho V_x A \\ \rho V_t A \\ \rho E^0 A \end{bmatrix} \quad F = \begin{bmatrix} \rho V_x A \\ (P + \rho V_x^2) A \\ \rho V_x V_t A \\ \rho H^0 V_x A \end{bmatrix} \quad Q = \begin{bmatrix} 0 \\ F_x \\ F_\theta \\ SW \end{bmatrix}$$

The cross section area is calculated through the simple form $A = 2\pi r b$.

Source terms are added to represent the interactions between the blade rows and the flow, and are derived from the velocity triangles. The axial forces developed by the blades and the hub and shroud walls are represented by F_x , the circumferential forces by F_θ and the shaft work SW denotes the energy brought to the fluid by the blades.

STEADY SIMULATIONS

The accuracy of the simulations is highly dependent on the source terms in the equations, which are derived from empirical correlations, particularly those for the loss coefficient and the deviation angle. Different empirical correlations have been chosen for different flow conditions, such as normal forward flow, stalled flow and reversed flow (see table 1).

Table 1: Selected empirical correlations

	Loss coefficient	Deviation angle
Forward, unstalled flow	Reference loss coefficient: Koch and Smith model	Reference deviation angle: NASA method [15]
	Off-design loss coefficient: Creveling model [16]	Off-design deviation angle: Lieblein's model [15]
Stalled flow	Moses and Thomason loss model [17, 18]	Tauveron deviation angle model [13]
Reversed flow	Longley modified loss model [14, 19, 20]	Exit flow parallel to the stagger direction

The criteria for stall inception

The separation of boundary layers in compressors is not fully understood. There are several basic criteria to detect it, such as the incidence angle, the total pressure loss coefficient or the diffusion rate. Yocum reports that flow separation occurs at an incidence angle of 8 deg, while Longley and Hypes find that in a multistage compressor a stage can operate unstalled at mass flows much lower than the isolated clean-flow stall inception point [21]. Bloch and O'Brien suggest that the

pumping action of the downstream stages tends to prevent upstream flow separation and propose a modified criterion based on the location of each stage in the compressor [22]:

$$i_{stall} = 8^\circ + \frac{N_{total} - N_{current}}{N_{total} - 1} \Delta i \quad \Delta i = i_{first-stage} - 8^\circ \quad (2)$$

According to the results of Gamache on his three-stage compressor, the first stage stalled at 16 deg incidence angle [23]. It is assumed that this result is generally applicable; therefore, the bounds on the incidence angle for stall inception are 8 deg for the last stage and 16 deg for the first stage.

This criterion will only be applied to the rotor. As it has been stated, a jet-wake structure is formed during the stalled flow. O'Brien expects that this flow structure has not enough time to mix to a uniform flow before reaching the downstream stator [22]. Thus, it seems reasonable to expect that the downstream stator stalls if the rotor stalls.

The criterion for reversed flow

A negative value of the average axial velocity in the compressor will be applied to indicate reversed flow conditions. This can be explained by the fact that the transition from stalled flow to reversed flow is very fast and that all blade rows can switch to reversed flow simultaneously.

The source terms

The force source terms can be derived from the steady Euler equations, as following:

$$Q = Q_b + Q_g = \begin{bmatrix} 0 \\ F_{b,x} \\ F_{b,\theta} \\ SW \end{bmatrix}_s + \begin{bmatrix} 0 \\ F_{g,x} \\ F_{g,\theta} \\ 0 \end{bmatrix} \quad (3)$$

$$Q_g = \begin{bmatrix} 0 \\ F_{g,x} \\ F_{g,\theta} \\ 0 \end{bmatrix} = \begin{bmatrix} 0 \\ \frac{\rho V \theta^2 A}{r} \frac{\partial r}{\partial x} + P \frac{\partial A}{\partial x} \\ -\frac{\rho V_x V_\theta A}{r} \frac{\partial r}{\partial x} \\ 0 \end{bmatrix} \quad (4)$$

The Q_b presents the influences of the blade and the fluid viscosity, and Q_g presents the variations of meanline and flow section.

These steady forces $F_{b,x}$ and $F_{b,\theta}$ are calculated from the steady Euler momentum equations and distributed linearly inside the blade rows. The circumferential force is responsible for the shaft work [24], which is calculated by:

$$SW = \Omega r F_{\theta,s} \quad (5)$$

The equation solver

The computational domain is generated according to the real flow path and is discretized at mid span using a one-dimensional mesh. The mesh cells are distributed not only in

the non-bladed regions but also within the blade rows, to make sure that the flow is turned gradually, with the advantage that spurious reflections of pressure waves are eliminated when they pass through the blade rows.

The integral form of the 1D axisymmetric Euler equations is expressed on each control volume with the conservative variables located at the cell centers. A quadratic reconstruction scheme with an hybrid limiter is applied to extrapolate the variables at the interfaces. Numerical fluxes are based on Roe's flux difference splitting and the spatial integration is implemented through an upwind scheme. A time-marching procedure allows the system to evolve toward a stationary solution. Both explicit and implicit schemes are implemented. The explicit scheme is based on fourth-order Runge-Kutta algorithm. The implicit scheme is based on an Euler single-step forward in time differentiation. This implicit time-marching method is used for stationary simulations, allowing large local CFL numbers to speed up the calculation. The boundary conditions applied at the inlet and the outlet of the multistage compressor are shown in Table 2.

Table 2: Boundary conditions

	Inlet	Outlet
Forward flow	$P_{in}^0, T_{in}^0, \alpha$	P_{out}
Stalled flow	$P_{in}^0, T_{in}^0, \alpha$	P_{out}
Reversed flow	P_{out}	$P_{in}^0, T_{in}^0, \alpha$

The reliability of the numerical results is verified by varying the number of grid cells and the time step and by checking the independency of the results.

TEST-CASE

The three-stage, low speed research axial compressor of Gamache was chosen because of the detailed geometry information and the available steady experimental results [23]. The steady-state pressure ratio for every stage and the overall performance are provided by Gamache and Estland for all flow regions. This compressor rig consists in three non-repeating stages with an inlet guide vane. The flow path is characterized by a constant mean radius and a constant annulus area. The mesh generated for this compressor is displayed in figure 1.

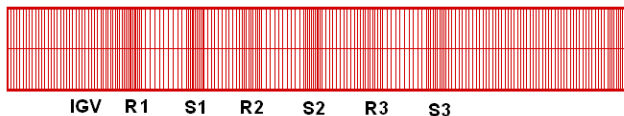


Figure 1: 1D mesh for the compressor of Gamache

During the numerical calculation, the throttle is gradually turned down in order to obtain a steady operating point in the

stalled region, while the reversed flow is achieved by imposing the appropriate boundary conditions (see table 2). The comparison of the numerical results and the experimental data are presented in figure 2.

It should be emphasized that the empirical correlations introduced into the model play a critical role for the accuracy of the simulations and that all correlations mentioned in the paper come from the open literature. These correlations may not give an accurate prediction for a particular compressor; however, they can capture the major flow features for all flow regions. As far as these correlations can be replaced by a manufacturer's own correlations, this simulation tool would certainly be able to provide better predictions. Meanwhile, further comparisons with other compressors will be carried out in the future to validate the empirical correlations used in this model.

TRANSIENT SIMULATIONS

A fourth-order Runge-Kunta method is used for time integration. However, for transient simulations of rotating stall and surge, the blade forces extracted from (steady) empirical correlations are not adequate because the time needed for mature stall cells to develop can be very long, and compressor mass flow can significantly change during this period of time. A first order transient response model is applied on the blade forces to take account of this time lag, as used by many other researchers [5]:

$$\tau \frac{dF}{dt} + F = F_{ss} \quad (6)$$

The value of the time constant τ is approximated to be several rotor revolutions.

The overall performance comparison

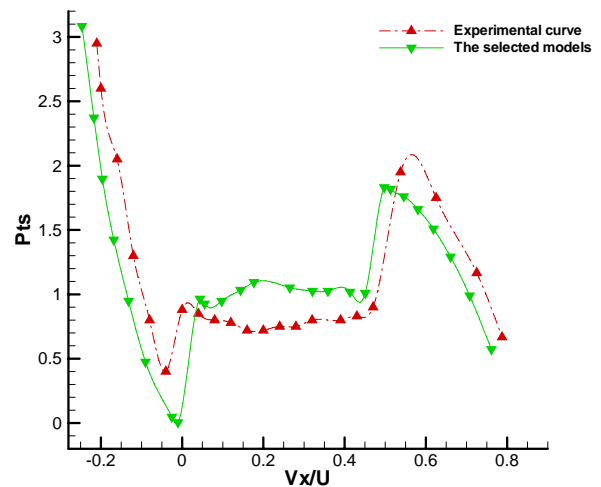


Figure 2: Comparison between selected models and experimental data in all flow regions

A throttle is represented at the outlet of the plenum, according to the following equation:

$$P = P_{ambient} + \frac{1}{2} K_{out} \rho V_x^2 \quad (7)$$

A characteristic method is implemented for the boundary conditions in order to avoid numerical spurious reflections. For positive flow operation the stagnation pressure and temperature are imposed as inlet boundary conditions, and ambient pressure is applied at the outlet boundary. In reversed flow operation, it seems unreasonable to expect surrounding air to flow back into plenum through the throttle, even though the fluid can enter the compressor duct from the plenum, and ambient pressure is always fixed at the outlet boundary. Meanwhile, it is likely that the flow can be discharged from the compressor through the inlet duct [12]. Therefore the ambient pressure is imposed at the inlet when the inlet velocity becomes negative, otherwise the stagnation pressure and temperature are imposed.

The same three-stage axial compressor of Gamache is used as a test case. It should be noted that transient experimental results are not available for this compressor, but experimental data from Greitzer [5] on a similar compressor can be taken as a reference. The transient simulations need the empirical correlations to replace the steady compressor characteristic, however, the transient results are not affected by the empirical correlations once the latter have been validated in steady calculations.

A plenum and a throttle are added to the compressor to form the compression system. A typical mesh is shown in figure 3.

Greitzer introduced a parameter $B = \frac{U}{2a} \cdot \sqrt{V_p / (A_c L_c)}$ to determine whether rotating stall or surge may occur in a particular compression system. In the numerical simulations, different volumes of the plenum, different compressor lengths and different rotating speeds have been selected in order to vary the values of this parameter B. The throttle is gradually turned down to approach the instability point.

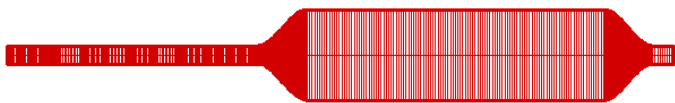


Figure 3: Typical mesh of the compression system

Rotating stall

It was stated that rotating stall is a 2D phenomenon which includes a strong non-axisymmetric distribution of mass flow and pressure. Although the present model is based on the axisymmetric assumption, it is still possible to predict the overall performance when the rotating stall is fully developed [22]. Since empirical correlations can estimate annular average performance through the blade rows, average pressure ratio and mass flow can be predicted.

The plenum is designed to obtain $B=0.45$. This is somewhat different compared to the experiment of Greitzer which is conducted for $B=0.65$ [5], since compressor rigs are different. Day proposed a modified parameter B to take account of the influence of steady characteristics [25]. In figures 4 and 5, average pressure coefficient versus time and average pressure coefficient versus average flow coefficient are shown.

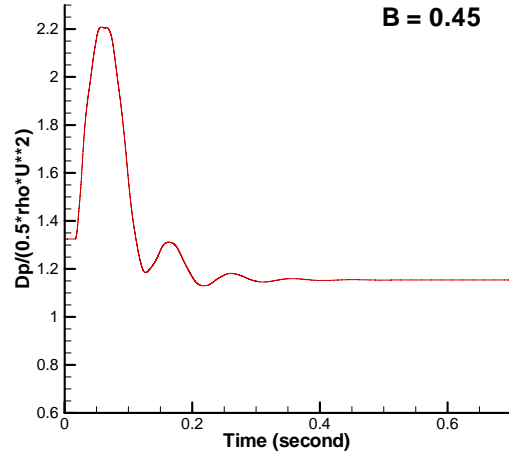


Figure 4: Average pressure coefficient versus time

In figure 4, it can be seen that the pressure ratio reaches a constant value after 0.35s of simulated time. In figure 5, a steady operating point is obtained with a significant drop of pressure ratio and mass flow coefficient after several small cycles, which indicates a fully developed rotating stall.

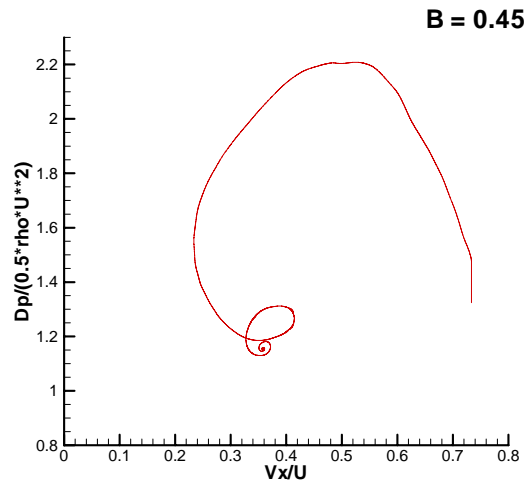


Figure 5: Average pressure coefficient versus the average mass flow coefficient

Classic surge

Three different compression systems (configurations 1, 2 and 3) are selected to obtain the same value $B=1.0$, by combining different compressor lengths, plenum volumes and rotating speeds (see table 3), in order to observe their influences on the shape of the surge cycles and on the

oscillation frequency. The plenum volume is modified by its length only, its section being kept constant.

Table 3: Different configurations for $B = 1.0$

Config	Plenum volume [m ³]	Compressor length [m]	RPM	Frequency [Hz]
1	4.481	0.508	1968	4.55
2	15.760	1.800	1968	1.30
3	1.908	0.508	3017	6.67

Figures 6 to 8 show the oscillations of pressure coefficient versus time in the middle of the plenum and mass flow versus time at the inlet and at the outlet of the plenum, for the three different geometrical configurations. It can be seen that the pressure coefficient in the plenum increases when the inlet mass flow is higher than the outlet one, otherwise the pressure decreases. The magnitude of the pressure oscillations are similar for the three configurations. However, the frequencies are quite different, the highest for configuration 3 and the lowest for configuration 2. This can be explained by the fact that the relevant time scale of the flow motion is characterized by the Helmholtz resonator frequency $\omega = U / 2BL_c$ [4] (see also figure 12).

Figure 9 shows a comparison of the shape of the surge cycles for these three configurations, characterized by the same value of $B = 1.0$. Similar surge cycles are obtained, which leads to the conclusion that a compression system exhibits a similar transient behavior for the same value of B , no matter how this value is achieved [5].

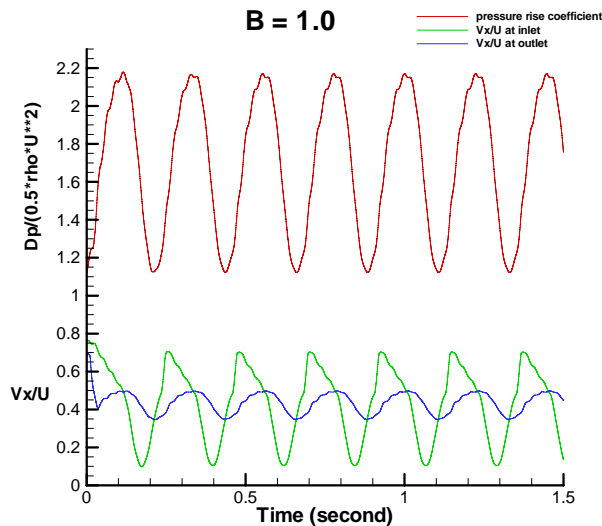


Figure 6: Evolution of the pressure and mass flow coefficients (configuration 1)

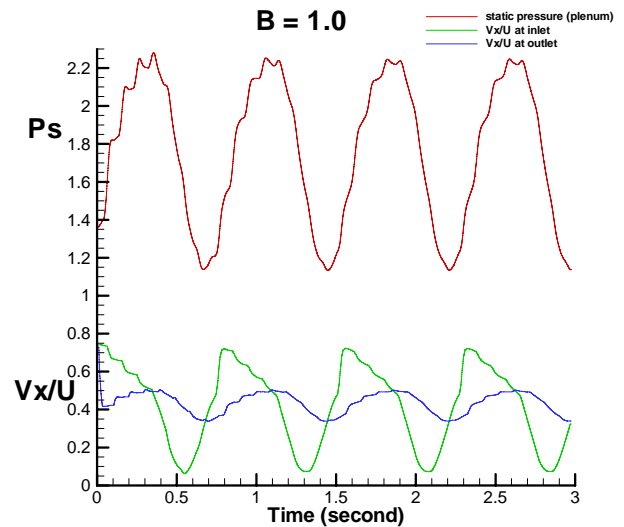


Figure 7: Evolution of the pressure and mass flow coefficients (configuration 2)

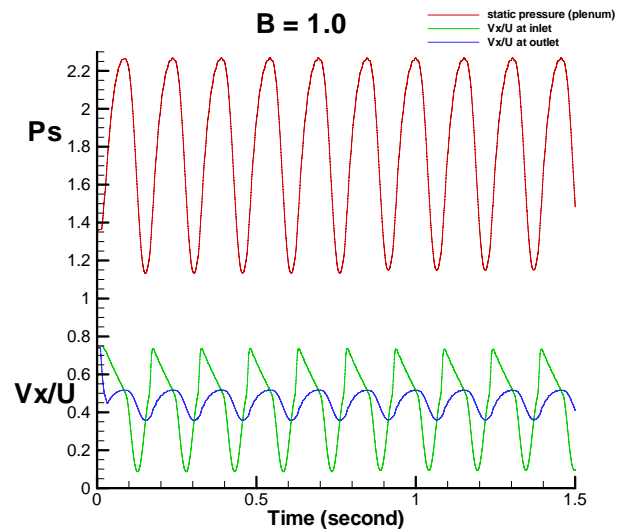


Figure 8: Evolution of the pressure and mass flow coefficients (configuration 3)

In order to observe the transient behavior for different values of B during classic surge, the volume of the plenum is adjusted in order to obtain a fourth configuration characterized by a higher parameter B . The compressor length and the rotating speed are kept constant. Configuration 4 is compared to configuration 1 in table 4.

Figure 10 shows the surge cycles obtained with different values of B . It can be seen that the surge cycles flatten with larger excursions in mass flow when B is increased. In figure 11, the pressure oscillations in the plenum are illustrated for different values of B . The frequency becomes lower with higher values of B , and this can also be explained by the Helmholtz resonator frequency during classic surge as shown in figure 12.

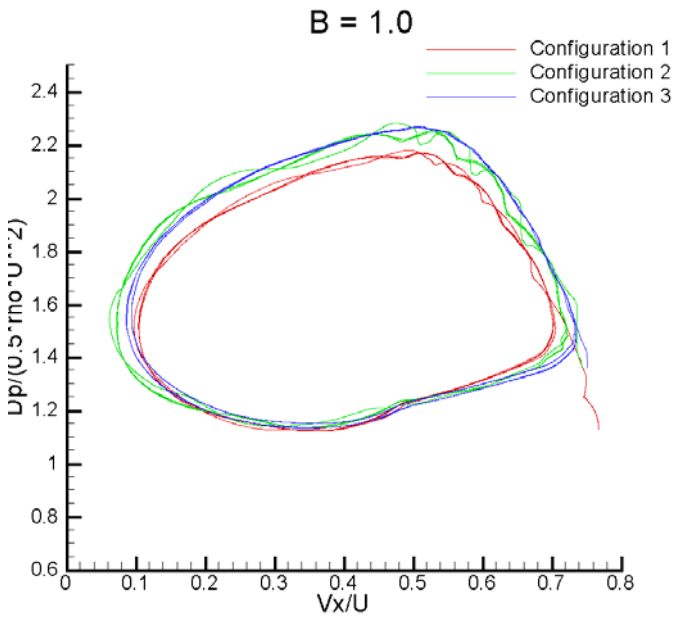


Figure 9: Shapes of surge cycles for different configurations

Table 4: Different configurations of the compression system
RPM=1968

Config	Plenum volume [m ³]	Compressor length [m]	B	Frequency [Hz]
1	4.481	0.508	1.01	4.55
4	5.964	0.508	1.12	3.57

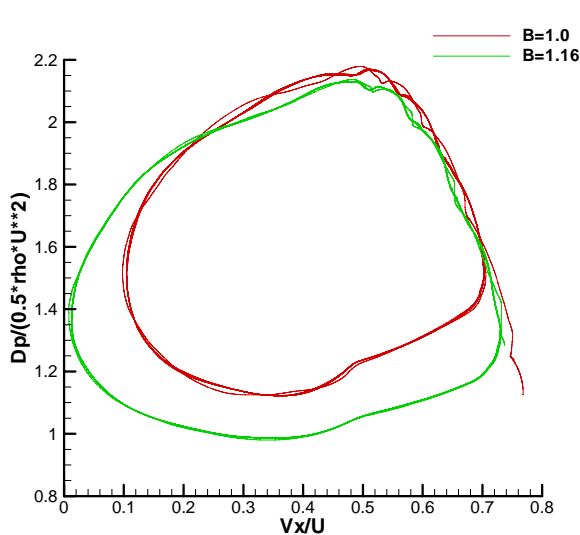


Figure 10: Shape of the surge cycles for different B

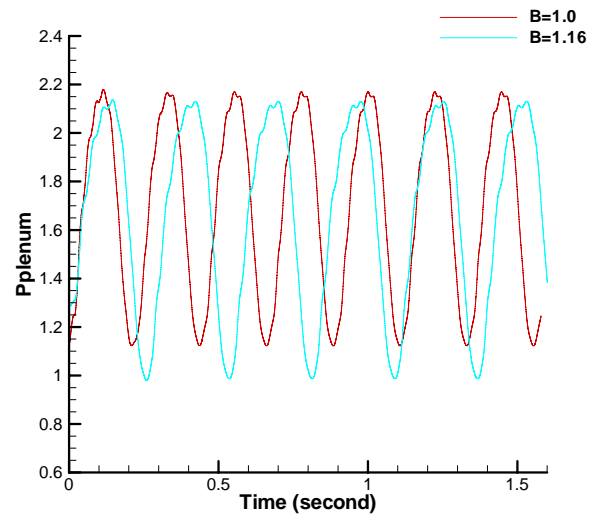


Figure 11: Pressure oscillations in plenum for different B

Configurations 1, 2, 3 and 4 were implemented to observe the surge transient behaviour; the relationship between the frequency and the Helmholtz resonator frequency was analyzed. The Helmholtz resonator frequency for configuration 1 is assumed as the reference value and the Helmholtz frequencies for configurations 2, 3 and 4 are calculated by $\omega = U / 2BL_c$. In figure 12, the surge frequency is found to be linear to Helmholtz resonator frequency for all configurations, as expected [4,5].

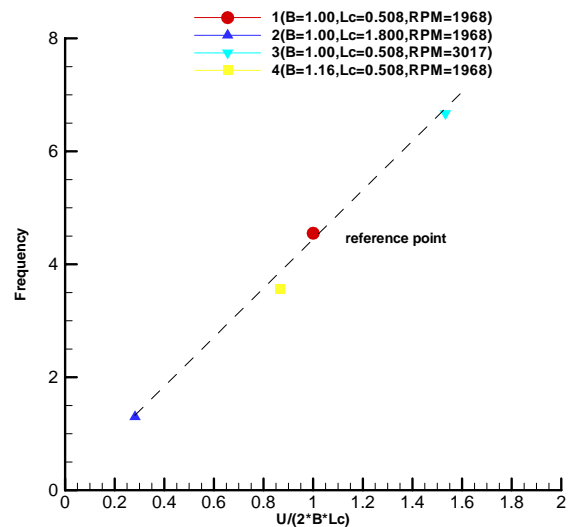


Figure 12: Relationship between frequency and Helmholtz resonator frequency for different configurations (classic surge)

Deep surge

As B continues to increase, the compression system exhibits a deep surge behavior, which is characterized by the occurrence of reversed flow in the compressor. The compression system is configured to obtain a value of $B=1.54$ and the throttle is gradually turned down to approach the instability point ($K_{out}=7.8$).

Figure 13 shows the pressure coefficient versus time in the plenum, and the mass flow coefficient at the inlet and at the outlet of the plenum versus time. As it was obtained for classic surge, the pressure coefficient is directly related to the net mass flux through the plenum.

Figure 14 indicates the location of the five stations simulated in the numerical tests. In figure 15 the mass flow coefficients at these five stations are presented. It can be seen that the evolution of the flow coefficient in the compressor duct (stations 1, 2 and 3) becomes of relaxed type; the evolution of the flow coefficient at the throttle (station 5) is of quasi-sinusoidal form while the mass flow coefficient in the plenum (station 4) changes a little.

During deep surge, the mass flow oscillation inside the compressor duct is not characterized by the Helmholtz resonator frequency, but includes two different time scales: the longest one corresponds to the mass flow which varies gradually when the plenum is built up (or emptied), and the shortest one corresponds to the mass flow which changes quite fast after the instability onset or when it recovers from the rotating stall. This is quite physical compared to the experimental results [5]. The mass flow coefficient at the throttle is mainly determined by the pressure difference between the plenum and the ambient pressure. Since the latter is constant, the evolution of the mass flow coefficient at the throttle follows the pressure in the plenum, which is quasi-sinusoidal (see figure 15). Because the section of the plenum is 15 times higher than in the compressor duct, the velocity in the plenum is much lower and the variations are rather small.

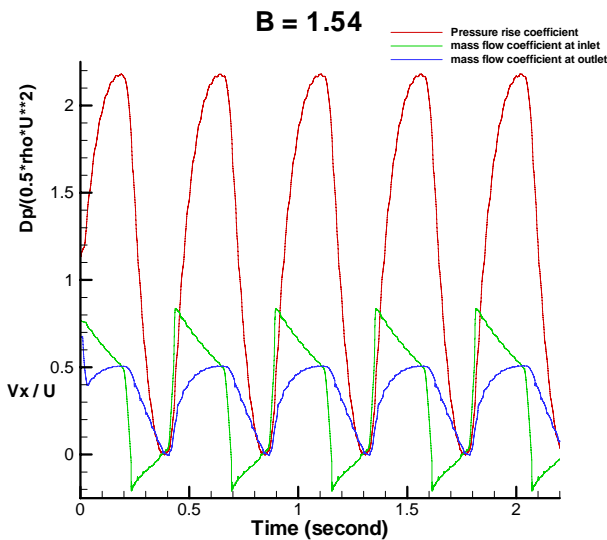


Figure 13: Pressure and mass flow coefficients for deep surge

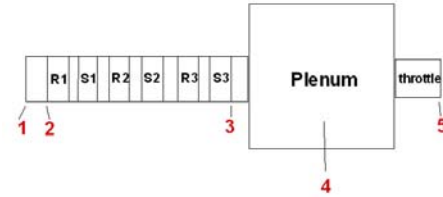


Figure 14: Simulated stations in the compression system

In figure 16, the static pressure in the five different locations are displayed. During the reversed flow, the static pressure drops dramatically at stations 3, 4 and 5, while it increases rapidly at station 1. The high pressure fluid of the plenum is discharged through the throttle and through the compressor at reversed flow, which leads to the fast pressure drop in the plenum and to the pressure increase at the compressor inlet. The pressure difference between stations 2 and 3 is created by the compressor that works as a high loss throttle device when the reversed flow passes through it. The static pressure at location 1 is constant because ambient pressure is imposed as the boundary condition once the velocity becomes negative.

In figure 17, the simulated surge cycle is compared to the experimental steady performance.

In order to observe the influence of the throttle setting during deep surge, the throttle is further closed ($K_{out}=15.0$). The surge cycles corresponding to two different throttle settings but the same compression system configuration and rotating speed are displayed in figure 18. The higher pressure ratio from instability point to reversed flow is caused by the fact that, by further turning down the throttle, the fluid inside the plenum becomes harder to be discharged through it. Except for this region, the surge cycle is almost the same and it indicates that its shape is almost independent of the throttle setting.

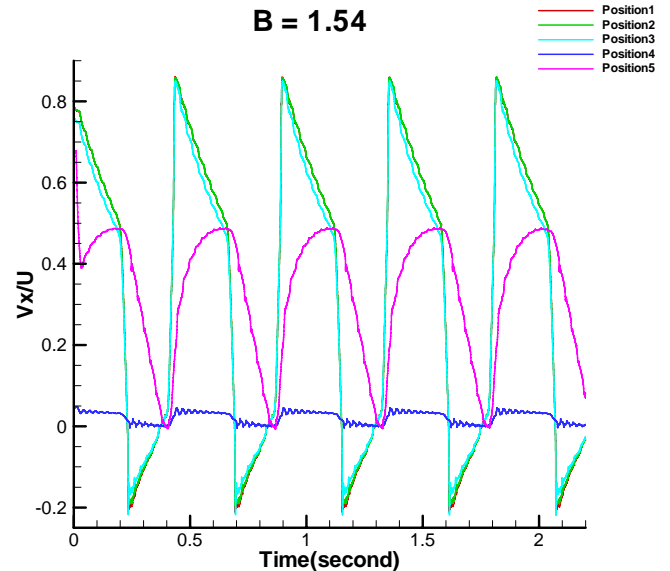


Figure 15: Flow coefficient versus time at five different stations during deep surge

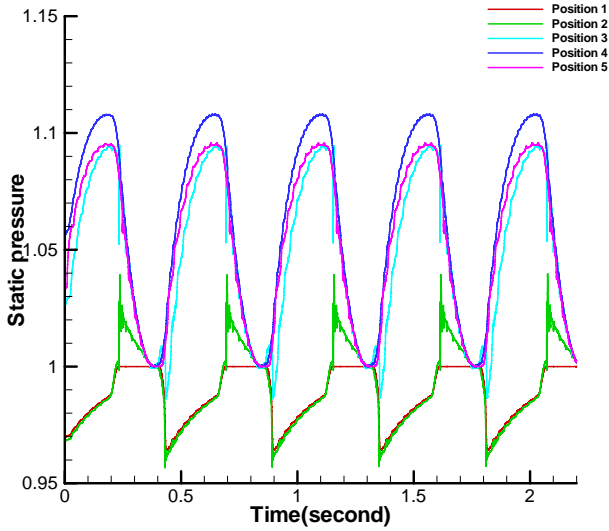


Figure 16: Static pressure versus time at different stations during deep surge

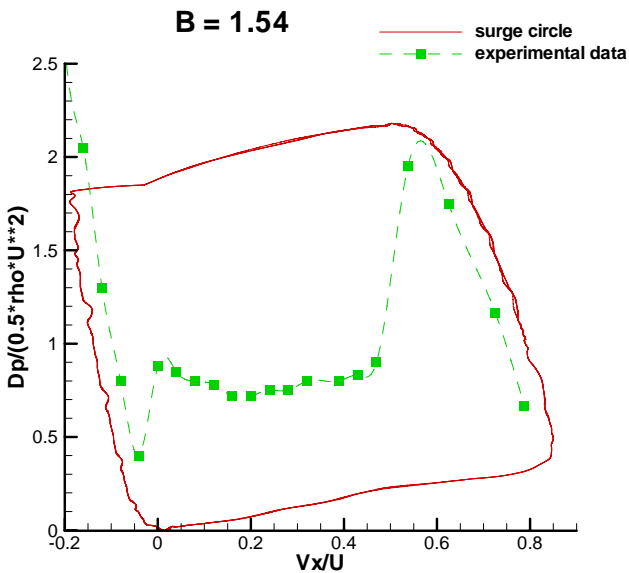


Figure 17: Comparison between simulated surge cycle and experimental steady data during deep surge

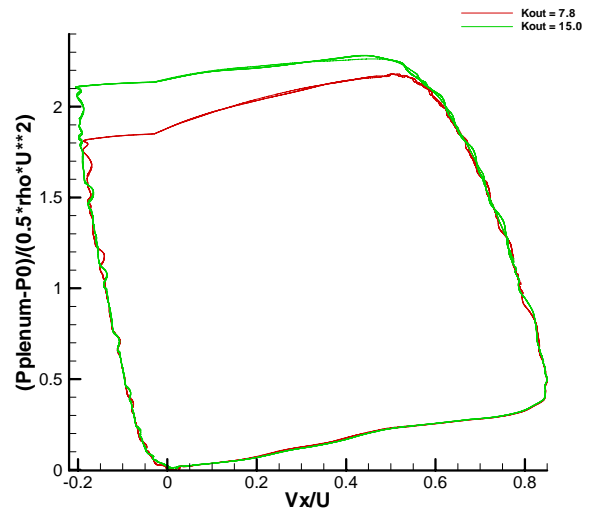


Figure 18: Shapes of surge cycles at different throttle settings

The comparison of the mass flow coefficients in the compressor for two different throttle settings is shown in figure 19. The ratio of the excursion region time between positive flow region and negative flow region for two throttle settings changes from $(T^+ / T^-)_{kout=7.8} = 2.25$ to $(T^+ / T^-)_{kout=15.0} = 1.21$.

When the throttle is turned further down, less time is needed to achieve the same instability point from a positive flow, while more time is required to dissipate the fluid in the plenum through the throttle and the compressor resistance during reversed flow. This is because the compressed fluid in the plenum is harder to be discharged through the throttle when further turned down. These numerical results follow a physical explanation, and similar results were found by Tauveron [12].

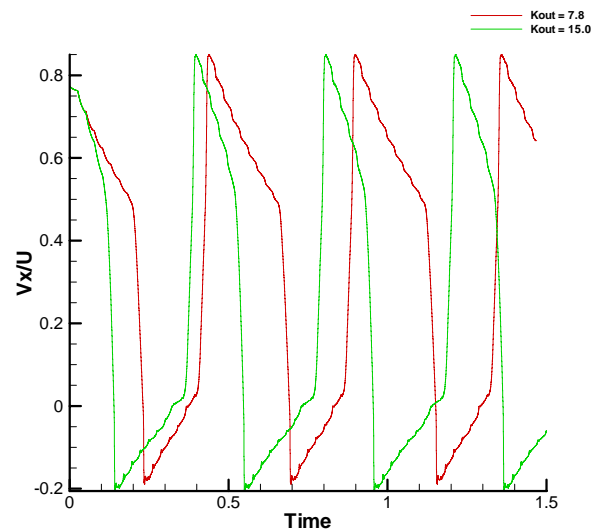


Figure 19: Mass flow coefficients for different throttle settings

CONTROL STRATEGY

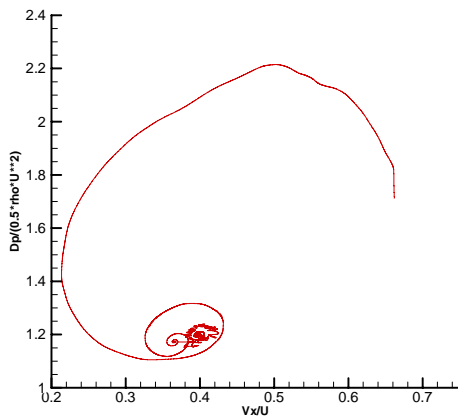
Aerodynamic instabilities including rotating stall and surge are major limitations of gas turbine engines. Control strategies are designed in order to obtain high performance and efficiency near the surge line.

Many studies have been carried out, focussing on feedback stabilization methods of compression systems, after the Moore-Greitzer model. Bleeding is regarded as a possible control device. This approach allows the compressor to shift from stall to normal operation. However the recoverability depends on the bleed location and on the bleed mass flow [22]. The influence of bleeding is easily introduced in the present model as additional source terms.

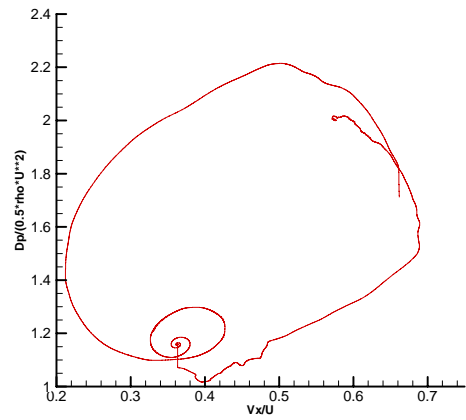
The compression system is configured with $B=0.5$ to test the influence of bleeding on rotating stall. The rotating stall takes place when the throttle is gradually turned down to the instability point; from there the throttle is kept unchanged. The bleed is alternatively located at an interstage or at the end of the plenum, and is opened once the rotating stall is developed maturely; the bleed mass flow is imposed as 15% of the unstalled mass flow [22]. All boundary conditions are identical except the bleed location.

Figure 20 shows the pressure coefficient versus the flow coefficient, and figure 21 the flow coefficient versus time, for different bleed locations. The results can be summarized as follows. The compressor does not recover from rotating stall when the bleed is located at an interstage, as shown in figure 20 (a). Actually the bleed increases the axial velocity of the upstream stage so that the incidence is reduced and it recovers from stall. However the downstream stages are not affected by the bleed and continue to be stalled as shown in figure 21 (a). Rotating stall is still present, with a slight increase of the overall mass flow and the pressure rise.

When the bleed is located at the end of the plenum, all stages recover from rotating stall as shown in figure 21 (b). However, when the compressor reaches a stable normal flow,



(a) the bleed is located between stator 1 and rotor 2



(b) the bleed is located at the end of plenum

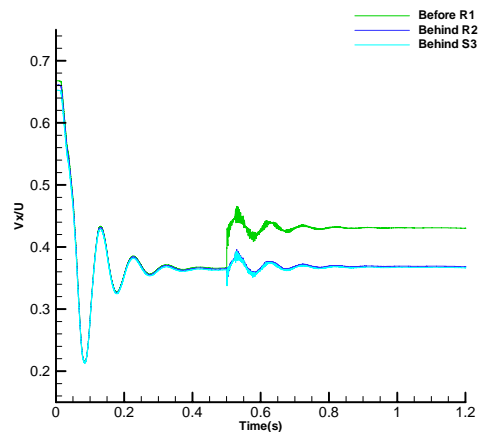
Figure 20: Pressure coefficient versus flow coefficient for different bleed locations

the pressure rise is much lower than the value without bleeding as in figure 20 (b).

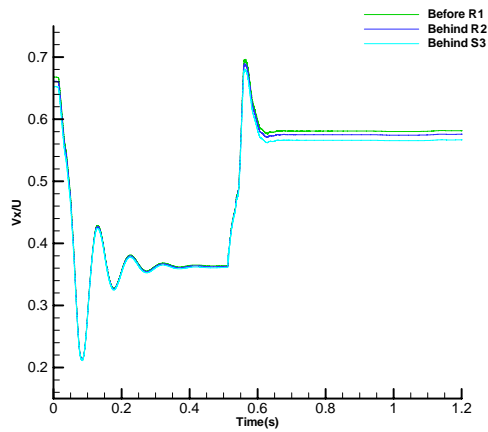
In another test, the same configuration as used for deep surge ($B=1.54$) is used, and a bleed is added to observe the influence on recoverability during surge. The bleed is located behind the plenum and 15% of the unstalled mass flow is applied. The bleeding action is activated after 1 simulated second, after several surge cycles. Figure 22 indicates that the compressor reaches a stable unstalled operating point after the bleeding action is applied.

CONCLUSIONS

A reliable prediction tool based on an adapted version of the 1D Euler equations with additional source terms has been developed and implemented to simulate the dynamic performance and the post-stall behavior of compression systems.



(a): the bleed is located between stator 1 and rotor 2



(b): the bleed is located at the end of plenum

Figure 21: Flow coefficient versus time for different bleeding locations

This model can be used for preliminary design purpose as it is based only on the compressor geometry: the blade angles at mid span and the hub and shroud geometry. The model does not rely on existing experimental performance curves nor on generic ones.

The empirical correlations provide a satisfactory prediction of the steady performance; however further validations using other compressor configurations are needed.

For rotating stall, the average pressure and mass flow coefficients can be predicted by the current quasi-one-dimensional model, provided that the rotating stall is fully developed.

For classic surge, different geometrical configurations have been selected to study the shape of the surge cycles and the frequency of the surge oscillations. It can be concluded that the shape of the surge cycle mainly depends on the parameter B and that the frequency of the surge is characterized by the Helmholtz resonator frequency.

For deep surge, the evolution of mass flow and pressure coefficients indicates that the compressor works as a high loss throttling device during the reversed flow. Meanwhile different throttle settings have been tested. The shape of the surge cycle is almost independent of the throttle setting and the ratio of the time excursion between positive flow and negative flow decreases when the throttle is further turned down.

A bleeding control strategy has been implemented to study the recoverability from rotating stall and surge. The effectiveness of the bleeding depends on its location and on the bleed mass flow.

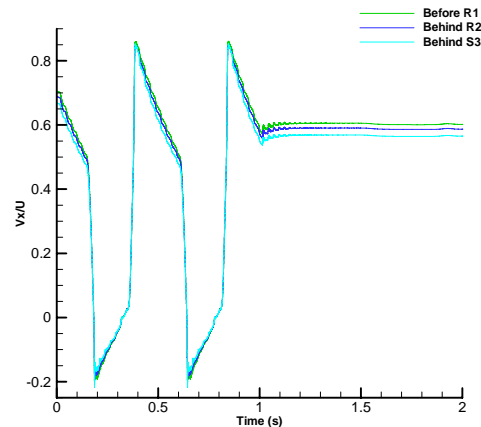
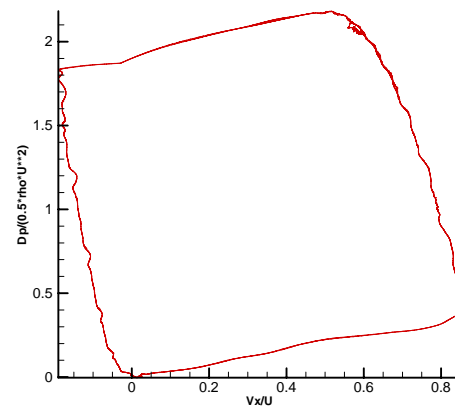


Figure 22: Surge cycle and mass flow coefficient versus time for different implementations of bleeding

REFERENCES

- [1] Adam O., and Léonard O., "A Quasi-One-Dimensional Model for Axial Compressors", 17th ISABE Conference, Munich, Germany, 2005
- [2] Gamache R.N., "Axial Compressor Reverse Flow Performance", PhD thesis, MIT, 1987
- [3] Greitzer E.M., "Review – Axial Compressor Stall Phenomena", Journal Fluids Eng., Vol. 102, 1980
- [4] Greitzer E.M., "Surge and Rotating Stall in Axial Flow Compressors. Part I: Theoretical Compression System Model", Journal of Engineering for Power, Vol. 100, 1978
- [5] Greitzer E.M., "Surge and Rotating Stall in Axial Flow Compressors. Part II: Experimental Results and Comparison with Theory", Journal of Engineering for Power, Vol. 100, 1978
- [6] Davis M.W., "A Stage-by-stage Post-stall Compression System Modeling Technique: Methodology, Validation, and Application", PhD thesis, 1987, Virginia Polytechnic Institute and State University
- [7] Morini M., "Development of A One-dimensional Modular Dynamic Model for Simulation of Surge in Compression Systems", Journal of Turbomachinery, Vol. 129, 2007

- [8] Takata H. and Nagato S., "Nonlinear Analysis of Rotating Stall", *Journal of Engineering for Power*, 1972
- [9] Moore F.K. and Greitzer E.M., "A Theory of Post-stall Transients in Axial Compression System: Part I: Development of Equations", ASME paper 85-GT-171
- [10] Longley J. P., "Calculating the Flowfield Behaviour of High-speed Multi-stage Compressors", ASME paper 97-GT-468
- [11] Lindau J.W. and Owen A.K.O., "Nonlinear Quasi-Three-Dimensional Modeling of Rotating Stall and Surge", AIAA paper 97-2772
- [12] Garnier V. and Escuret J.F., "Numerical Simulations of Surge and Rotating Stall in Multi-stage Axial-flow Compressors", AIAA paper 94-3202
- [13] Tauveron N., Saez M., Ferrand P. and Leboeuf, F., "Axial Turbomachine Modeling with a 1D Axisymmetric Approach. Application to Gas Cooled Nuclear Reactor", *Nuclear Engineering and Design* 237 (2007) 1679-1692
- [14] Longley J.P., "Calculating Stall and Surge Transients", ASME paper GT-2007-27378
- [15] Lieblein S., "Experimental Flow in Two-Dimensional Cascades", NASA SP-36, 1965
- [16] Creveling H.F. and Carmody, "Axial-Flow Compressor Computer Program for Calculating Off-design Performance", NASA-CR-72472, 1968
- [17] Moses H.L., Thomason S.B., "An Approximation for Fully Stalled Cascades", AIAA TN Vol. 2, No 2
- [18] Day I.J., Greitzer E.M., Cumpsty N.A., "Prediction of Compressor Performance in Rotating Stall", *ASME Journal of Engineering for Power*, Vol. 100, 1978
- [19] Gamache R.N. and Greitzer E.M., "Reverse Flow in Multistage Axial Compressors", AIAA paper 86-1747
- [20] Tauveron N., "Simulation numérique et analyse du déclenchement et du développement des instabilités axiales dans les turbomachines. Application à un transitoire de brèche dans un réacteur nucléaire à hélium", PhD thesis, Ecole Centrale de Lyon, 2006
- [21] Longley J.P. and Hynes T.P., "Stability of Flow Through Multistage Axial Compressors", *Journal of Turbomachinery*, Vol. 112(1), 1990
- [22] O'Brien W. F., "Dynamic Simulation of Compressor and Gas Turbine Performance", AGARD LS-183
- [23] Gamache, R.N., "Axial Compressor Reverse Flow Performance", PhD thesis, MIT, 1987
- [24] Chima R.V., "A Three-dimensional Unsteady CFD Model of Compressor Stability", NASA TM 2006-214117, 2006
- [25] Day I.J., "Axial Compressor Performance During Surge", *AIAA Journal of Propulsion and Power*, Vol. 10, No. 3, 1994